

Novel Dark Matter Models and Detection Strategies

Jason Kumar

Department of Physics and Astronomy, University of Hawaii, Honolulu, HI, 96822 USA

Abstract. We consider the impact of relaxing some typical assumptions about dark matter interactions, including isospin-invariance, elastic scattering and contact interactions. We show that detection strategies with neutrino detectors, gamma-ray searches, new direct detection experiments and collider searches can all provide complementary information. We argue that data from many such strategies may be necessary to gain a more complete understanding of dark matter interactions.

Keywords: dark matter

PACS: 95.35.+d

INTRODUCTION

The idea that experiments could search for dark matter beyond its gravitational effects was proposed almost 30 years ago [1]. Since that time, the search for dark matter has become an experimental reality, and dark matter research is a field which is well beyond its infancy. Data is arriving from a variety of detectors using different strategies, and some very interesting hints which may suggest the presence of dark matter have been seen.

WIMPs of the MSSM are one of the most appealing dark matter candidates, and dark matter search results are often interpreted with this model in mind. Aside from the theoretical appeal of LSP WIMPs, this model is relatively constrained, bringing with it a number of assumptions which simplify the tasks of interpreting the data and comparing data from different detectors. Typical assumptions which one makes include:

- *Isospin-invariance:* It is assumed that dark matter interactions with protons and neutrons are the same.
- *Elastic interactions:* It is assumed that dark matter scatters elastically off nuclei.
- *Contact interactions:* It is assumed that dark matter-nucleon interactions are mediated by a very heavy particle.
- *Single component:* It is assumed that all dark matter consists of a single new particle, the MSSM LSP.

But as new data comes in, and potential hints of dark matter are seen by some detectors, it has becoming increasingly clear that it may be difficult to reconcile the data from all of these experiments under the assumptions given above. It is thus necessary to consider how the role of different detection strategies changes when the above assumptions are relaxed.¹ We will argue that, in the absence of the above assumptions, it is necessary to combine the results of several experiments using novel detection strategies in order to study the nature of dark matter interactions.

DARK MATTER INTERACTIONS

It is useful to briefly review the general structure of non-relativistic dark matter-nucleus scattering. We allow for the possibility that the outgoing dark sector particle may have a mass $m_{X'}$ which is different from the dark matter mass m_X (we will assume $m_{X'} \geq m_X$). But since we assume that both incoming and outgoing particles are non-relativistic, we have $\delta m_X \equiv m_{X'} - m_X \ll m_X$. We may then write the reduced mass as $\mu_A = m_X m_A / (m_X + m_A)$ for both the incoming and outgoing system, where m_A is the nucleus mass. For cold dark matter, one expects dark matter to coherently scatter off the nucleus as a whole. The dark matter-nucleus differential scattering cross-section is

$$\frac{d\sigma}{dE_R} = \frac{\mu_A P_{out}}{16\pi m_X^2 m_A^2 v} \left(\frac{1}{N_{spins}} \sum |\mathcal{M}|^2 \right) |F_A(E_R)|^2 \frac{1}{E_+ - E_-} \theta(E_+ - E_R) \theta(E_R - E_-), \quad (1)$$

¹ Dynamical dark matter [2], where dark matter is not a single component, is considered elsewhere in these proceedings.

where v is the relative velocity of the incoming particles, $p_{out} = \mu_A v \sqrt{1 - 2\delta m_X / \mu_A v^2}$ is the outgoing momentum in center of mass frame, \mathcal{M} is the matrix element for dark matter-nucleus scattering, N is the number of initial states, and the sum is over all initial and final states. The nuclear form factor is given by $F_A(E_R)$, and the maximum (minimum) nucleus recoil energy which is kinematically possible in two-body scattering is given by E_+ (E_-):

$$E_{\pm} = \frac{\mu_A^2 v^2}{m_A} \left(1 - \frac{\delta m_X}{\mu_A v^2} \pm \sqrt{1 - \frac{2\delta m_X}{\mu_A v^2}} \right) = \frac{\mu_A v}{m_A} \left[\mu_A v \left(1 - \frac{\delta m_X}{\mu_A v^2} \right) \pm p_{out} \right]. \quad (2)$$

The differential rate of scattering events is then given by [3]

$$\frac{dR}{dV} = \eta_T \eta_X \int d^3u f(u) \frac{v^2}{u} \int_{E_{min}}^{E_+} dE_R \frac{d\sigma}{dE_R}, \quad (3)$$

where $\eta_{T,X}$ are the number densities of the target material and of dark matter, respectively. The dark matter velocity distribution is given by $f(u)$, where u is the velocity of a dark matter particle relative to the detector when it is far from the solar system. Note that u and v can be different, since an infalling dark matter particle will gain speed before scattering due to the gravitational potential; we then have $(1/2)m_X(v^2 - u^2) = |V_{grav}(r)|$, where $V_{grav}(r)$ is the gravitational potential energy of the dark matter at r . Usually $u \approx v$, unless scattering occurs within the sun. The lower integration limit is given by $E_{min} = \max[E_{th}, E_-]$, where E_{th} is the threshold recoil energy.

Thus far we have relied only on kinematics, making no assumptions about dark matter particle physics. Henceforth, we will focus only on the case where dark matter interactions are spin-independent. In that case, the dark matter coupling scales as the number of nucleons and $\mathcal{M} \propto [f_p Z + f_n(A - Z)]$, where $f_{p,n}$ parameterize the relative strength of dark matter interactions with protons and neutrons, respectively. If scattering arises through exchange of a single mediating particle with mass M_* , then we may write the matrix element as

$$\mathcal{M} = \frac{G(m_X, m_A, s, t, u)}{q^2 - M_*^2} [f_p Z + f_n(A - Z)], \quad (4)$$

where G is a dimension-2 function of the masses and Mandelstam variables. The momentum transfer in the hard scattering process, q , is give by $q^2 \sim m_X^2$, $-2m_A E_R$, m_X^2 for s -, t - and u -channel exchange, respectively. For t -channel exchange, the shape of the recoil spectrum will depend on whether the propagator is dominated by the messenger mass or the momentum transfer. Since $|t| < 4m_A^2 v^2$, scattering interactions will be short-ranged if $M_* \gtrsim 1$ GeV.

We will also assume that scattering is velocity-independent, which is the case if there are no cancelations in the leading order term of the matrix element. G is determined, up to coupling constants and other numerical factors, by the normalization of the incoming and outgoing states and by the derivatives (if any) in the matrix element. We find that $G \propto m_X m_A$ for fermionic dark matter, or for scalar dark matter which couples to the mediating particle through a derivative. For scalar dark matter (examples include [4]) without a derivative coupling, we can also have terms of the form $G \propto M_* m_A$.

If dark matter scatters elastically, then we may set $\delta m_X = 0$. If $|t| \ll M_*^2$, then we may write

$$\frac{d\sigma^{Z,A}}{dE_R} = \frac{\mu_A^2}{M_*^4} [f_p Z + f_n(A - Z)]^2 |F_A(E_R)|^2 \frac{\theta(E_+ - E_R)}{E_+} = \frac{\sigma^p}{E_+} \frac{\mu_A^2}{\mu_p^2} \left[Z + \frac{f_n}{f_p} (A - Z) \right]^2 |F_A(E_R)|^2 \theta(E_+ - E_R), \quad (5)$$

where μ_p is the dark matter-proton reduced mass and σ^p is the dark matter-proton spin-independent scattering cross-section. One can make motivated assumptions about η_X , $f(u)$ (from astrophysics) and $F_A(E_R)$ (from nuclear physics). The only parameter left is f_n/f_p ; given a choice of this parameter, a bound on the event rate can be directly translated into a bound on σ^p . Conversely, an excess event rate can be directly translated into a preferred region for σ^p .

ISOSPIN-VIOLATING DARK MATTER

Typically, bounds are presented in terms of a “normalized-to-nucleon” scattering cross-section, σ_N^Z . This is the dark matter-nucleon scattering cross-section which would be inferred under the assumption $f_n = f_p$, and provides an easy way to compare the results of experiments using different targets. But the quantity which actually should agree among different experiments is the dark matter-proton scattering cross-section, σ^p , which is related to σ_N^Z by the relation

$$\frac{\sigma^p}{\sigma_N^Z} \equiv F_Z = \frac{\sum_i \eta_i \mu_{A_i}^2 A_i^2}{\sum_i \eta_i \mu_{A_i}^2 [Z + (A_i - Z) f_n / f_p]^2}. \quad (6)$$

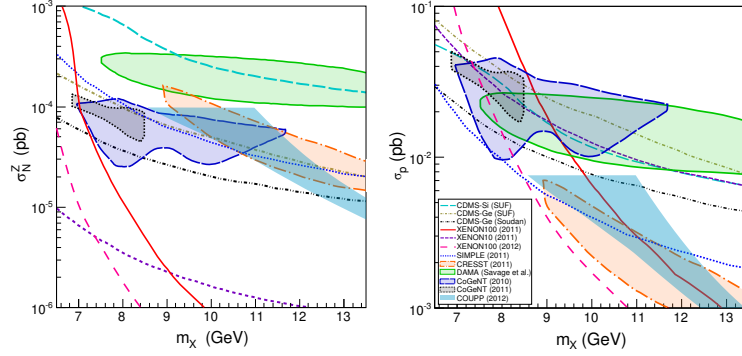


FIGURE 1. Favored regions and exclusion contours in the (m_X, σ_N^Z) plane (left), and in the (m_X, σ_p) plane for IVDM with $f_n/f_p = -0.7$ (right). (Figure courtesy of David Sanford.)

The sum is over isotopes labeled by i , and η_i is the natural abundance of the i th isotope (we have assumed that $F_{A_i}(E_R)$ does not vary much between isotopes). F_Z thus depends only on f_n/f_p , and as expected, $F_Z = 1$ for $f_n/f_p = 1$. For isospin-violating dark matter (IVDM) [5, 6], f_n/f_p is a parameter which is set by the details of the particle physics model. Figure 1 [6] shows the favored regions of DAMA [7, 8] (3σ), CoGeNT [9, 10] (90% CL) and CRESST [11] (2σ), and 90% CL exclusion contours from CDMS [12, 13], XENON10 [14], XENON100 [15, 16, 17], SIMPLE [18] and COUPP [19]. The left panel plots these regions for $f_n/f_p = 1$, while the right panel assumes $f_n/f_p = -0.7$.

One can see the dramatic effect of isospin-violating interactions on the relative sensitivity of various direct detection experiments. For $f_n/f_p = -0.7$, the CoGeNT and DAMA preferred regions are brought closer into alignment, while the bounds from XENON10/100 are weakened, and no longer exclude the entire DAMA and CoGeNT regions. However, it is clear that this is not a complete solution. The marginal tension between bounds from CDMS (Soudan) and the preferred region of CoGeNT is not altered by isospin-violating interactions, since both detectors use a germanium target. Moreover, although the choice $f_n/f_p = -0.7$ would alleviate the tension with the xenon-based experiments, it creates tension with bounds from the SIMPLE experiment. And there is no choice of f_n/f_p for which the signal regions from DAMA, CoGeNT and CRESST are all consistent.

There are many experimental uncertainties with the data at low-mass, some of which will be resolved soon. CoGeNT is gaining a better understanding of their surface-area contamination [20], which will likely move their preferred signal region to higher mass and lower cross-section. The understanding of the response of sodium and xenon-based detectors to low-energy recoils is improving. New germanium-based (Majorana, SuperCDMS) and xenon-based (LUX) detectors will soon provide even higher sensitivity at low-mass. It seems clear that the possibility of isospin-violating interactions will have a significant impact on the interpretation of this new data.

If one treats f_n/f_p as a free parameter of the particle physics model, then one finds that one must use multiple direct detection experiments to get a handle on dark matter interactions. We may define the ratio

$$R[Z_1, Z_2](f_n/f_p) \equiv \frac{F_{Z_2}}{F_{Z_1}} = \frac{\sigma_N^{Z_1}}{\sigma_N^{Z_2}}, \quad (7)$$

which is the ratio of normalized-to-nucleon cross-sections which would be inferred by two detectors, using materials with Z_1 and Z_2 protons, under the assumption of isospin-invariant interactions. Signals at two dark matter experiments provide an experimental measurement of R and can be used to solve for f_n/f_p . If a detector using a material with Z_1 protons finds a dark matter signal, $R[Z_1, Z_2]$ determines the range of sensitivity a second detector (using a material with Z_2 protons) would need to either potentially confirm or definitively exclude this signal for any choice of f_n/f_p .

If an element has multiple isotopes, no choice of f_n/f_p can result in total destructive interference between proton and neutron couplings for all isotopes. For example, marginalizing over f_n/f_p , we find $\max\{R[Z_1 = Ge, Z_2 = Xe](f_n/f_p)\} \sim 22$; a xenon-based detector would need at most a factor of 22 greater sensitivity to confirm a signal at a germanium-based detector, for any choice of f_n/f_p . Data from LUX could thus provide a much more definitive test of the signals from DAMA, CoGeNT and CRESST, assuming the low-energy response can be well understood.

Although IVDM is often discussed in relation to low-mass dark matter, it is a possibility which one must consider for any dark matter signal. Figure 2 [21] shows the sensitivities of XENON1T [22], Super-CDMS [23], MiniCLEAN,

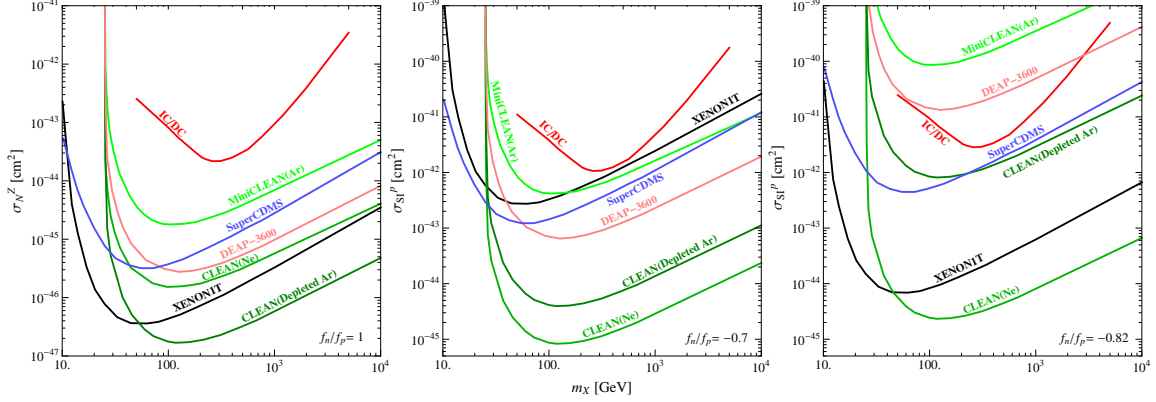


FIGURE 2. Sensitivity to σ^P for $f_n/f_p = 1$ (left panel), $f_n/f_p = -0.7$ (center panel) and $f_n/f_p = -0.82$ (right panel) for IC/DC with 180 days of data, and for other labeled experiments (see text).

DEAP-3600 and CLEAN [24], for $f_n/f_p = 1, -0.7$, or -0.82 . Also plotted in figure 2 is the estimated sensitivity of IceCube/DeepCore [25] with 180 days of data (assuming annihilation to the hard channel).

Dark Matter Searches with Neutrino Detectors

IceCube/DeepCore and other neutrino detectors search for the neutrino flux arising from dark matter annihilation in the core of the sun. If the sun is in equilibrium, bounds on the dark matter annihilation rate can be directly translated into bounds on the rate at which dark matter is captured by the sun through scattering off solar nuclei.² In turn, this yields a bound on the dark matter-proton scattering cross-section. The dark matter capture rate can also be derived from eqn. 3, where the threshold energy E_{th} is the minimum recoil energy needed for dark matter to be captured.

Dark matter capture occurs when a dark matter particle scatters and loses enough energy to become confined to an orbit around the sun. After many subsequent scatterings, it will eventually settle to the core of the sun, where it annihilates. But since many-body effects can be important for dark matter in large-radius orbits, one often requires captured dark matter to be confined to an orbit which will not exceed a maximum distance r_0 from the sun (typically taken to be the Jupiter-sun distance). The minimum recoil energy necessary for capture is thus given by

$$E_{th} = \max \left[\frac{1}{2} m_X (u^2 + v_{esc.}(r_0)^2) - \delta m_X, 0 \right], \quad (8)$$

where $v_{esc.}(r_0)$ is the escape velocity for a particle at distance r_0 from the sun.

One can then determine the capture rate from scattering against each element by integrating the differential capture rate (eq. 3) throughout the volume of the sun, accounting for the densities of different elements, as well as the sun's gravitational potential. If one computes the capture rate for each isotope of each element under the assumption of isospin-invariant interactions, then one obtains the capture rate for any choice of f_n/f_p by simply rescaling by the factor $[Z + (f_n/f_p)(A - Z)]^2/A^2$.

As shown in figure 2, when there is destructive interference between proton and neutron scattering, neutrino detectors can provide a nice complementary probe with a sensitivity which is comparable to that of direct detection experiments. This is because many direct detection experiments use heavy nuclei which have many more neutrons than protons; scattering in the sun is largely off lighter elements (including hydrogen), with fewer neutrons.

Neutrino detectors can also provide sensitivity to low-mass dark matter which is comparable to that of direct detection experiments [26, 27, 28]. This can easily be understood from eq. 3. For $m_X \sim 5 - 10$ GeV many direct detection experiments satisfy $m_X \ll m_A$, $E_+ \sim 2m_X^2 v^2/m_A$, $E_{th} = \text{fixed}$, implying that the event rate vanishes for small

² This bound also depends on the neutrino spectrum produced by dark matter annihilation; we assume annihilation only to $\bar{\nu}\nu$ for $m_X \leq 80$ GeV, and annihilation only to W^+W^- for $m_X > 80$ GeV.

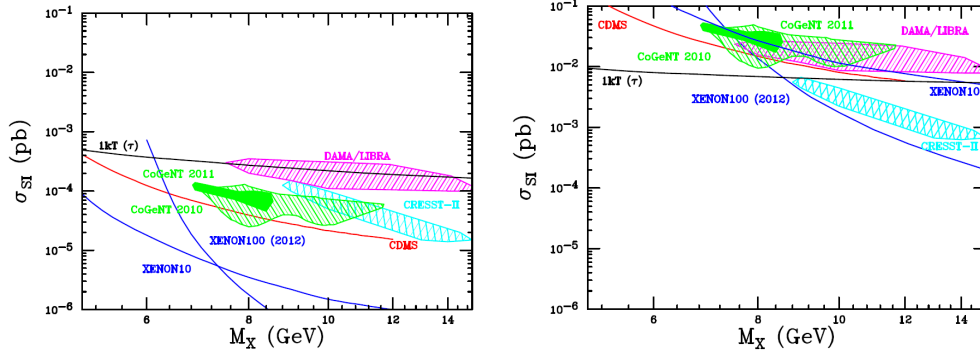


FIGURE 3. Favored regions and exclusion contours in the (m_X, σ_p) plane for $f_n/f_p = 1$ (left) and for IVDM with $f_n/f_p = -0.7$ (right). (Figure courtesy of Stefanie Smith.)

m_X . For neutrino detectors, however, there are many relatively light elements with mass comparable to the dark matter, implying $E_+ \sim 2m_X v^2$, while $E_{th} = (1/2)m_X u^2 < E_+$. In fact, neutrino detectors can be sensitive to dark matter as light as 4 GeV; lighter dark matter will evaporate out of the sun [3].

We will consider a search for dark matter annihilation utilizing a 1 kT liquid scintillation (LS) detector with 2135 live-days of data (roughly the specifications of KamLAND). Neutrino detectors search for the charged lepton produced from $\bar{\nu}, \nu$ by a charged-current interaction. It has recently been realized that LS detectors can also be used for dark matter searches, because the direction of the charged lepton track in the scintillator can be determined from the timing of the first photons reaching the PMTs [29]. Moreover, the charged lepton flavor can be determined with very high efficiency. For low-energy ν_μ (arising from low-mass dark matter annihilation), the muons produced by a charged-current interaction will be short-ranged; there is thus no great advantage in searching for muons which may have been produced outside the detector volume. Instead, we focus on a search for e^\pm produced from electron (anti-)neutrinos, which have the advantage of a much smaller atmospheric neutrino background.

In figure 3 [27] we plot the sensitivity which can be achieved with KamLAND's current data set (assuming annihilation to $\bar{\tau}\tau$), as well as the DAMA, CoGeNT and CRESST signal regions and the CDMS, XENON10 and XENON100 exclusion curves, assuming $f_n/f_p = 1, -0.7$. We can see that KamLAND, with its current data set, can potentially probe the signals of DAMA and CoGeNT if $f_n/f_p \sim -0.7$.

Complementary Bounds from Indirect Detection and the LHC

Indirect detection and collider bounds provide interesting complementary tests of IVDM models. The $Xq \rightarrow Xq$ scattering matrix element is related to the $XX \rightarrow \bar{q}q$ annihilation matrix element and the $\bar{q}q \rightarrow XX$ production matrix element by crossing symmetry. As a result, if an assumption is made about the form and flavor dependence of the scattering matrix element, then bounds on the total annihilation cross-section $\langle \sigma_{A\bar{A}} \rangle$ or on the production cross-section can be directly translated into a bound on σ^p . The sensitivity of direct detection experiments using heavy targets, such as xenon, is minimized for the case of partial destructive interference between f_n and f_p . In that case, a signal seen at CoGeNT corresponds to a large value of σ^p ($\mathcal{O}(10^{-2})$ pb). This implies a large coupling to up- and down-quarks, which destructively interfere. The dark matter annihilation cross section to up- and down-quarks, or production cross-section from $\bar{q}q$ initial states, can then be greatly enhanced. A key point to note, though, is that the kinematics of these complementary processes can be different. For the annihilation process, the momentum transfer is roughly $2m_X$, while for the production process, the momentum transfer is typically $> 2m_X$.

We will consider the case where dark matter-nucleus scattering is spin- and velocity-independent, and arises from tree-level t -channel exchange with quarks. Furthermore, we will only consider the case where the resulting annihilation matrix element is not p -wave suppressed. For scalar dark matter (real or complex), these conditions are only satisfied by exchange of a scalar, while for Dirac fermion dark matter one must exchange a vector (these conditions can thus not be satisfied for Majorana fermion dark matter). In Table 1, we list the energy dependence of the scattering, annihilation and creation matrix elements, as well as the effective scattering operator in the limit where scattering is a contact interaction ($|t| \ll M_\pi^2$). If we assume that dark matter couples only to up- and down-quarks in the limit of elastic

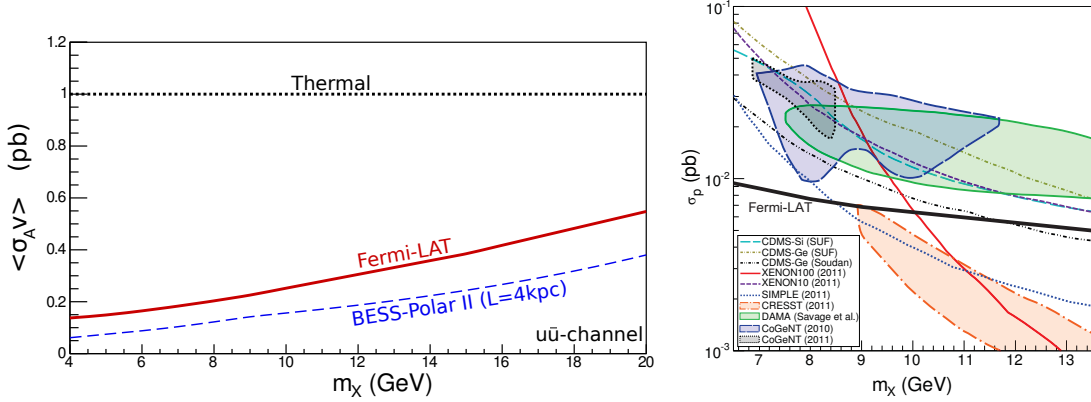


FIGURE 4. The left panel shows bounds on the annihilation cross-section $\langle\sigma_A v\rangle$ from Fermi data and from BESS-Polar II. The dashed line labeled “Thermal” is at $\langle\sigma_A v\rangle = 1$ pb. The right panel shows favored regions and exclusion contours for the labeled experiments in the (m_X, σ_p) plane for IVDM with $f_n/f_p = -0.7$. The solid black line is the 95% CL bound from Fermi-LAT data.

contact scattering, then for any given choice of the contact operator and f_n/f_p , we can directly relate the annihilation and production cross-sections to the scattering cross-section.

Fermi-LAT Searches of Dwarf Spheroidals

Tight bounds can be placed on dark matter annihilation in dwarf spheroidal galaxies with data from the Fermi-LAT [30, 31]. These bounds can be phrased in terms of the quantity

$$\Phi_{PP} \equiv \frac{\langle\sigma_A v\rangle}{8\pi m_X^2} \int_{E_{thr}}^{m_X} \sum_f B_f \frac{dN_f}{dE} dE, \quad (9)$$

where σ_A is the total annihilation cross-section and B_f and dN_f/dE are the branching fraction and photon spectrum, respectively, for annihilation to final state f . For a threshold energy $E_{thr} = 1$ GeV, the 95% CL bound is $\Phi_{PP} \leq 5.0^{+4.3}_{-4.5} \times 10^{-30} \text{cm}^3 \text{s}^{-1} \text{GeV}^{-2}$ [31], where the uncertainties in the bound arise from systematic uncertainties in the density profile of the dwarf spheroidal galaxies.

We computed dN_f/dE for low-mass dark matter annihilation to the up- and down-quark channels (the two channels are essentially identical) using the Hawaii Open Supercomputing Center (HOSC). The corresponding bounds on $\langle\sigma_A v\rangle$ are plotted in the left panel of figure 4 [32], along with bounds from BESS-Polar II measurements of the anti-proton flux [33]. Systematic uncertainties can weaken these Fermi bounds by up to a factor of 2, or strengthen them by up to a factor of 10. In contrast, BESS-Polar II bounds may be weakened by up to a factor of 50 [34] due to systematic uncertainties in cosmic ray propagation, solar modulation, etc.

These bounds can be directly translated into bounds on σ^p , under the assumption $|t|, m_X^2 \ll M_*^2$. For the case when dark matter is a complex scalar ($f_n/f_p \sim -0.7$), these bounds are plotted in the right panel of figure 4. If dark matter is a real scalar or Dirac fermion, then these bounds are tightened by a factor of 2 or ~ 4 , respectively.

TABLE 1. Contact operators (arising from t -channel exchange) which permit spin-independent, velocity-independent scattering and s -wave annihilation. Also listed are the energy dependence of the scattering, annihilation and production matrix elements.

particle	exchange	contact operator	$\mathcal{M}_{Xq \rightarrow Xq}$	$\mathcal{M}_{XX \rightarrow \bar{q}q}$	$\mathcal{M}_{\bar{q}q \rightarrow XX}$
complex scalar	scalar	$\mathcal{O}_C = (1/M_*) X^* X \bar{q} q$	$\propto \frac{M_* m_X}{t - M_*^2}$	$\propto \frac{M_* m_X}{4m_X^2 - M_*^2}$	$\propto \frac{M_* \sqrt{s_{prod.}}}{s_{prod.} - M_*^2}$
real scalar	scalar	$\mathcal{O}_R = (1/M_*) X^2 \bar{q} q$	$\propto \frac{M_* m_X}{t - M_*^2}$	$\propto \frac{M_* m_X}{4m_X^2 - M_*^2}$	$\propto \frac{M_* \sqrt{s_{prod.}}}{s_{prod.} - M_*^2}$
Dirac fermion	vector	$\mathcal{O}_D = (1/M_*^2) \bar{X} \gamma^\mu X \bar{q} \gamma_\mu q$	$\propto \frac{m_X m_A}{t - M_*^2}$	$\propto \frac{m_X^2}{4m_X^2 - M_*^2}$	$\propto \frac{s_{prod.}}{s_{prod.} - M_*^2}$

We can see that these constraints would rule out an IVDM model which could match the DAMA and CoGeNT data. But this is subject to the specific assumptions which we have made. For example, if dark matter couples to up-

TABLE 2. Upper bounds on σ^p from ATLAS monojet searches, assuming the listed cuts on the leading jet p_T and on the missing transverse energy. The columns correspond to Dirac fermions, complex scalars, and real scalars respectively.

m_X	\mathcal{O}_D	\mathcal{O}_C	\mathcal{O}_R		m_X	\mathcal{O}_D	\mathcal{O}_C	\mathcal{O}_R
4 GeV	0.00285 pb	90.6 pb	181 pb		4 GeV	0.00079	10.8 pb	21.6 pb
7 GeV	0.00320 pb	35.4 pb	70.3 pb		7 GeV	0.00092	4.2 pb	8.50 pb
10 GeV	0.00357 pb	18.9 pb	37.6 pb		10 GeV	0.00097	2.3 pb	4.51 pb
15 GeV	0.00370 pb	9.1 pb	18.2 pb		15 GeV	0.00106	1.1 pb	2.13 pb
20 GeV	0.00380 pb	5.4 pb	10.9 pb		20 GeV	0.00107	0.62 pb	1.24 pb

(a) $p_T > 120$ GeV
 $\cancel{E}_T > 120$ GeV

(b) $p_T > 350$ GeV
 $\cancel{E}_T > 300$ GeV

and down-quarks through an elastic contact operator which permits spin-independent, velocity-independent scattering, but only p -wave suppressed annihilation, then models which could potentially match the DAMA and CoGeNT data would be unconstrained by Fermi bounds. Another possibility is that dark matter may couple to Standard Model matter through a relatively light mediator with mass $M_* \sim 1$ GeV. In this case, scattering interactions would still be short-ranged, but dark matter annihilation would have an additional $M_*^4/(2m_X)^4 \ll 1$ suppression.

Monojet searches at the LHC

An interesting way to bound direct dark matter production is with monojet or monophoton searches at colliders [35, 36]. Much work has been done on this search strategy [37]. The key uncertainties in setting this bound arise from the flavor structure of dark matter-quark couplings, and the energy dependence of the $\bar{q}q \rightarrow XX$ matrix element. For example, if one assumes that the dark matter coupling to quarks is proportional to the quark mass, then a large contribution to the LHC event rate will typically come from couplings to $\bar{c}c$, $\bar{b}b$, even though these couplings yield a relatively small contribution to the scattering cross-section.

Similarly, if the matrix element scales with negative powers of the energy, the dark matter production cross-section at the LHC will also be suppressed, since the energy scale of the dark matter production process is $> 2m_X$ due to the phase space suppression at the production threshold. Fermionic dark matter is tightly constrained by LHC monojet/monophoton bounds, since the relativistic normalization of the dark matter state will introduce additional positive powers of the energy of the process, as seen in Table 1. On the other hand, models with $M_* \sim 1$ GeV will have negative powers of the process energy from the propagator, and are very weakly constrained.

In Table 2 [32], we indicate bounds on σ^p derived from ATLAS monojet searches ($pp \rightarrow XXj$) with 1 fb⁻¹ of data [35], if we assume dark matter couples only to first generation quarks through operators which permit elastic contact spin-independent velocity-independent scattering and s -wave annihilation. We assume $f_n/f_p = -0.7$. These bounds arise from analyses using two possible cuts on \cancel{E}_T and on the p_T of the leading jet, as listed. The bounds on scalar dark matter are not competitive, but bounds on Dirac fermion dark matter can be competitive with (and in some cases exceed) bounds from direct detection experiments and Fermi. However, if dark matter interacts through a low-mass mediator ($M_* \lesssim 1$ GeV), then bounds from the LHC will be weakened by several orders of magnitude.

LONG-RANGE INTERACTIONS

If dark matter scatters through a very low-mass mediator ($M_*^2 \ll 2m_A E_{th}$), then the differential scattering cross-section scales like $(2m_A E_R)^{-2}$ instead of M_*^{-4} . As a result, light elements will tend to have enhanced scattering cross-sections. For example, the event rate at neutrino detectors is expected to receive a significant enhancement relative to leading direct detection experiments, due to the presence of many light elements in the sun.

In the case of elastic long-range interactions, unlike elastic contact scattering, we cannot parameterize bounds on dark matter-nucleon scattering in terms of the total cross-section, which is infinite (an example is Rutherford scattering). Instead, we can parameterize the dark matter-nucleus differential scattering cross-section as:

$$\frac{d\sigma^{Z,A}}{dE_R} = C \frac{4\pi\alpha^2\mu_A^2}{m_A^2 E_R^2 E_+} \left[Z + \frac{f_n}{f_p} (A - Z) \right]^2 |F_A(E_R)|^2, \quad (10)$$

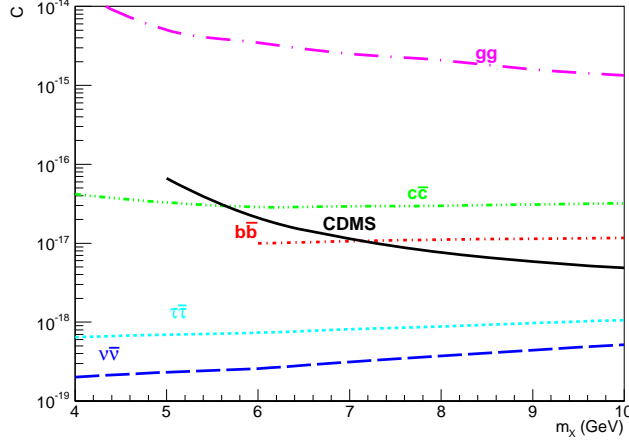


FIGURE 5. Sensitivity to C of CDMS and a 1 kT LS detector (2135 live days of data) for low-mass dark matter with isospin-invariant elastic long-range interactions. LS detector sensitivity is shown assuming annihilation to either the τ , b , c , g and ν (flavor-independent) channels.

where C is a constant which normalizes the strength of the mediator coupling to dark matter (g_X) and to the proton (g_p) to the proton charge; $C = g_X^2 g_p^2 / e^4$.

Figure 5 [28] shows the sensitivity of a 1 kT LS detector with 2135 days of data, assuming annihilation exclusively to either the τ , b , c , ν (flavor-independent) or g channels. The neutrino spectra arising from dark matter annihilation to these channels was simulated using the HOSC cluster. We also plot the estimated sensitivity of CDMS, if their current bounds are reinterpreted as bounds on long-range dark matter interactions. Note that the CDMS sensitivity is derived under the assumption that the detector's efficiency is constant above the threshold; as a result of these and other assumptions [28], the CDMS sensitivity curve should only be regarded as an estimate. Nevertheless, it is clear that neutrino detectors have a sensitivity to dark matter models with long-range interactions which can rival leading direct detection experiments. A detector with a 51 kT liquid argon target [38] could achieve the same sensitivity as that given in figure 5 with ~ 17 days of data.

INELASTIC DARK MATTER (IDM)

If dark matter scattering is inelastic [39], then neutrino detectors can provide interesting detection possibilities which are complementary to direct detection experiments. For iDM, we again cannot characterize the bounds from experiments in terms of the dark matter-nucleon scattering cross-section, because there are kinematic regimes where dark matter-nucleon scattering is forbidden, while dark matter can still scatter off heavier elements. The reason is easy to see; for inelastic scattering to occur, the total initial kinetic energy in center-of-mass frame must exceed δm_X . This yields the constraint $(1/2)\mu_A v^2 > \delta m_X$, and as m_A decreases, v must increase in order for this constraint to be satisfied.

We can instead parameterize the dark matter-nucleus differential scattering cross-section as

$$\frac{d\sigma^{Z,A}}{dE_R} = \frac{m_A I}{32\pi v^2} \left[Z + \frac{f_n}{f_p}(A - Z) \right]^2 |F_A(E_R)|^2, \quad (11)$$

where the squared dark matter-nucleus scattering matrix element can be written as $m_X^2 m_A^2 [Z + (A - Z)(f_n/f_p)]^2 |F_A(E_R)|^2 \times I$. I is a quantity which, at leading order, is thus independent of the target nucleus mass and the relative velocity.

In figure 6 [28] we plot the dark matter capture rate as a function of m_X (in the low-mass regime) for $I/32\pi = 10^{-4}$ pb GeV $^{-2}$, for each element in the sun. As expected, we see that, as δm_X increases, the capture rate from scattering off light elements decreases. Interestingly, we find that the capture is significant even for relatively large δm_X . Indeed, dark matter capture in the sun is possible even for values of δm_X which would render inelastic scattering on earth kinematically impossible. The reason is that dark matter gains significant kinetic energy as it falls towards

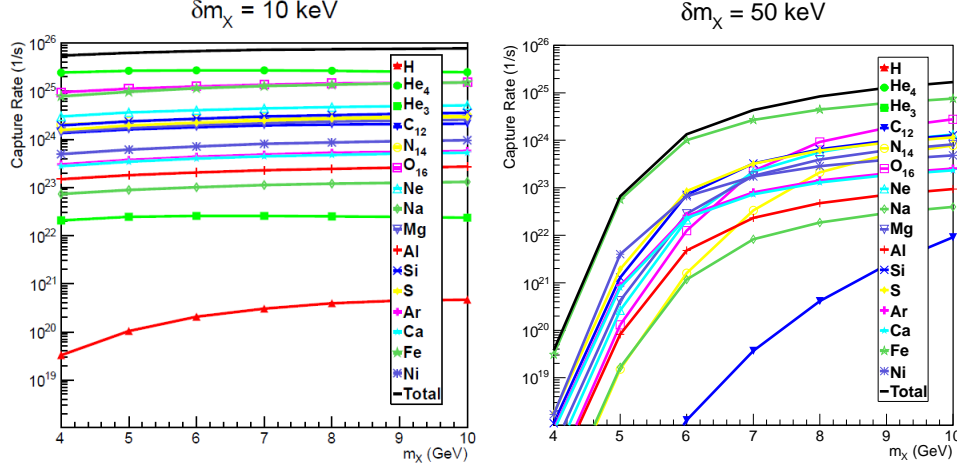


FIGURE 6. Dark matter capture rates for various elements in the sun, assuming isospin-invariant inelastic elastic contact interactions with $\delta m_\chi = 10$ keV (left panel) and 50 keV (right panel). We set $I/32\pi = 10^{-4}$ pb GeV $^{-2}$.

the sun, allowing inelastic scattering even for large δm_χ . The escape velocity at the surface of the sun is ~ 600 km/s; one would expect the range of δm_χ accessible to neutrino detectors via dark matter capture in the sun to be roughly a factor of 10 larger than that accessible to earth-based direct detection experiments.

CONCLUSION

We have seen that, by relaxing some of the assumptions typically made regarding dark matter interactions, one can dramatically change the interpretation of data from direct detection, indirect detection and collider experiments. This suggests that, to gain a definitive understanding of the properties of dark matter, one may need to combine data from a variety of different detectors. Moreover, one finds that some reasonable dark matter models are best probed with novel detection strategies. Neutrino detectors, gamma-ray searches of dwarf spheroidal galaxies, and collider searches can all play an important complementary role.

All of these new possibilities for dark matter interactions have interesting implications for upcoming detectors. An illustrative example is the D³ experiment [40], which is under construction at the University of Hawaii. This experiment is a low-threshold gas time projection chamber which uses ionization to image the track made by a recoiling gas nucleus. An initial plan is for this detector to use a fluorocarbon target. One can thus see that, for IVDM models with destructive interference, detectors such as D³ can have enhanced sensitivity as compared to other direct detection experiments. For example, one can compare the normalized-to-nucleon cross-section which would be seen by a fluorine-based detector to that of a germanium-based detector if $f_n/f_p = -0.7$, in which case one finds $\sigma_N^{Z=F} = 4.2 \times \sigma_N^{Z=Ge}$. Another interesting possibility is the use of a hydrocarbon target. This could be especially interesting in the case where dark matter interactions are long-ranged. As we have seen, the squared scattering matrix element scales as m_A^{-2} in the case of long-range interactions, implying that a detector with a hydrogen target would receive an $\mathcal{O}(10^3)$ enhancement in sensitivity relative to a detector with a germanium target.

As more data comes in from a variety of current and upcoming experiments, it will be important to keep in mind the effect which relaxing typical theoretical assumptions can have on a coherent interpretation of the data.

ACKNOWLEDGMENTS

We are grateful to J. L. Feng, Y. Gao, D. Marfatia, K. Richardson, M. Sakai, D. Sanford, S. Smith and L. Strigari, for collaboration. We are grateful to HOSC and we thank the Center for Theoretical Underground Physics and Related Areas (CETUP* 2012) in South Dakota for its hospitality and for partial support during the completion of this work. This work is supported in part by the Department of Energy under Grant DE-FG02-04ER41291.

REFERENCES

1. M. W. Goodman and E. Witten, Phys. Rev. D **31**, 3059 (1985).
2. K. R. Dienes and B. Thomas, Phys. Rev. D **85**, 083523 (2012) [arXiv:1106.4546 [hep-ph]]; K. R. Dienes and B. Thomas, Phys. Rev. D **85**, 083524 (2012) [arXiv:1107.0721 [hep-ph]]; K. R. Dienes and B. Thomas, Phys. Rev. D **86**, 055013 (2012) [arXiv:1203.1923 [hep-ph]]; K. R. Dienes, S. Su and B. Thomas, Phys. Rev. D **86**, 054008 (2012) [arXiv:1204.4183 [hep-ph]]; K. R. Dienes, J. Kumar and B. Thomas, Phys. Rev. D **86**, 055016 (2012) [arXiv:1208.0336 [hep-ph]].
3. W. H. Press and D. N. Spergel, Astrophys. J. **296**, 679 (1985); A. Gould, Astrophys. J. **321**, 571 (1987).
4. N. G. Deshpande and E. Ma, Phys. Rev. D **18**, 2574 (1978); J. L. Feng, J. Kumar and L. E. Strigari, Phys. Lett. B **670**, 37 (2008) [arXiv:0806.3746 [hep-ph]]; S. Andreas, T. Hambye and M. H. G. Tytgat, JCAP **0810**, 034 (2008) [arXiv:0808.0255 [hep-ph]].
5. A. Kurylov and M. Kamionkowski, Phys. Rev. D **69**, 063503 (2004) [arXiv:hep-ph/0307185]; F. Giuliani, Phys. Rev. Lett. **95**, 101301 (2005) [arXiv:hep-ph/0504157]; S. Chang *et al.*, JCAP **1008**, 018 (2010) [arXiv:1004.0697 [hep-ph]]; Z. Kang, *et al.*, JCAP **1101**, 028 (2011) [arXiv:1008.5243 [hep-ph]].
6. J. L. Feng, *et al.*, Phys. Lett. B **703**, 124 (2011) [arXiv:1102.4331 [hep-ph]].
7. R. Bernabei, *et al.*, Eur. Phys. J. **C67**, 39-49 (2010). [arXiv:1002.1028 [astro-ph.GA]].
8. C. Savage *et al.* JCAP **0904**, 010 (2009) [arXiv:0808.3607 [astro-ph]]; C. Savage *et al.*, Phys. Rev. D **83**, 055002 (2011) [arXiv:1006.0972 [astro-ph.CO]].
9. C. E. Aalseth *et al.*, Phys. Rev. Lett. **106**, 131301 (2011) [arXiv:1002.4703 [astro-ph.CO]].
10. C. E. Aalseth *et al.*, Phys. Rev. Lett. **107**, 141301 (2011) [arXiv:1106.0650 [astro-ph.CO]].
11. G. Angloher *et al.*, [arXiv:1109.0702 [astro-ph.CO]].
12. D. S. Akerib *et al.*, Phys. Rev. D **82**, 122004 (2010) [arXiv:1010.4290 [astro-ph.CO]].
13. Z. Ahmed *et al.*, Phys. Rev. Lett. **106**, 131302 (2011) [arXiv:1011.2482 [astro-ph.CO]].
14. J. Angle *et al.*, Phys. Rev. Lett. **107**, 051301 (2011) [arXiv:1104.3088 [astro-ph.CO]].
15. E. Aprile *et al.*, Phys. Rev. Lett. **105**, 131302 (2010) [arXiv:1005.0380 [astro-ph.CO]].
16. E. Aprile *et al.*, Phys. Rev. Lett. **107**, 131302 (2011) [arXiv:1104.2549 [astro-ph.CO]].
17. E. Aprile *et al.* [XENON100 Collaboration], arXiv:1207.5988 [astro-ph.CO].
18. M. Felizardo, *et al.*, [arXiv:1106.3014 [astro-ph.CO]].
19. E. Behnke *et al.* [COUPP Collaboration], Phys. Rev. D **86**, 052001 (2012) [arXiv:1204.3094 [astro-ph.CO]].
20. C. E. Aalseth *et al.* [CoGeNT Collaboration], arXiv:1208.5737 [astro-ph.CO].
21. Y. Gao, J. Kumar and D. Marfatia, Phys. Lett. B **704**, 534 (2011) [arXiv:1108.0518 [hep-ph]].
22. See talk by D. Cline, <http://public.lanl.gov/friedland/info11/info11talks/ClineDM-INFO11.pdf>
23. See talk by T. Saab, <http://indico.in2p3.fr/contributionDisplay.py?sessionId=26&contribId=58&confId=1565>
24. See talk by R. Hennings-Yeomans, http://deapclean.org/talks/PHENO2011_Hennings.pdf
25. C. d. I. Heros [for the IceCube Collaboration], arXiv:1012.0184 [astro-ph.HE].
26. D. Hooper, *et al.*, Phys. Rev. D **79**, 015010 (2009) [arXiv:0808.2464 [hep-ph]]; J. L. Feng, *et al.*, JCAP **0901**, 032 (2009) [arXiv:0808.4151 [hep-ph]]; J. Kumar, J. G. Learned and S. Smith, Phys. Rev. D **80**, 113002 (2009) [arXiv:0908.1768 [hep-ph]]; A. L. Fitzpatrick, D. Hooper and K. M. Zurek, Phys. Rev. D **81**, 115005 (2010) [arXiv:1003.0014 [hep-ph]]; S. -L. Chen and Y. Zhang, Phys. Rev. D **84**, 031301 (2011) [arXiv:1106.4044 [hep-ph]].
27. J. Kumar, *et al.*, Phys. Rev. D **84**, 036007 (2011) [arXiv:1103.3270 [hep-ph]].
28. J. Kumar, *et al.*, arXiv:1204.5120 [hep-ph].
29. J. G. Learned, arXiv:0902.4009 [hep-ex]; J. Peltoniemi, [arXiv:0909.4974 [physics.ins-det]].
30. M. Ackermann *et al.* [Fermi-LAT Collaboration], Phys. Rev. Lett. **107**, 241302 (2011) [arXiv:1108.3546 [astro-ph.HE]].
31. A. Geringer-Sameth and S. M. Koushiappas, Phys. Rev. Lett. **107**, 241303 (2011) [arXiv:1108.2914 [astro-ph.CO]].
32. J. Kumar, D. Sanford and L. E. Strigari, Phys. Rev. D **85**, 081301 (2012) [arXiv:1112.4849 [astro-ph.CO]].
33. K. Abe *et al.*, Phys. Rev. Lett. **108**, 051102 (2012) [arXiv:1107.6000 [astro-ph.HE]]; R. Kappl and M. W. Winkler, arXiv:1110.4376 [hep-ph].
34. C. Evoli, *et al.*, Phys. Rev. D **85**, 123511 (2012) [arXiv:1108.0664 [astro-ph.HE]].
35. ATLAS Collaboration, ATLAS-CONF-2011-096.
36. S. Chatrchyan *et al.* [CMS Collaboration], Phys. Rev. Lett. **107**, 201804 (2011) [arXiv:1106.4775 [hep-ex]]; T. Aaltonen *et al.* [CDF Collaboration], Phys. Rev. Lett. **108**, 211804 (2012) [arXiv:1203.0742 [hep-ex]].
37. J. L. Feng, S. Su, F. Takayama, Phys. Rev. Lett. **96**, 151802 (2006) [hep-ph/0503117]; J. Goodman, *et al.*, Phys. Lett. **B695**, 185-188 (2011) [arXiv:1005.1286 [hep-ph]]; Y. Bai, P. J. Fox and R. Harnik, JHEP **1012**, 048 (2010) [arXiv:1005.3797 [hep-ph]]; J. Wang, *et al.*, Phys. Rev. D **84**, 075011 (2011) [arXiv:1107.2048 [hep-ph]]; A. Rajaraman, *et al.*, [arXiv:1108.1196 [hep-ph]]; J. Goodman, *et al.*, Phys. Rev. **D82**, 116010 (2010) [arXiv:1008.1783 [hep-ph]]; P. J. Fox, *et al.*, Phys. Rev. D **85**, 056011 (2012) [arXiv:1109.4398 [hep-ph]]; J. Goodman, W. Shephard, [arXiv:1111.2359 [hep-ph]].
38. T. Akiri *et al.* [LBNE Collaboration], arXiv:1110.6249 [hep-ex].
39. D. Tucker-Smith and N. Weiner, Phys. Rev. D **64**, 043502 (2001) [hep-ph/0101138]; D. Tucker-Smith and N. Weiner, Phys. Rev. D **72**, 063509 (2005) [hep-ph/0402065].
40. S. E. Vahsen, *et al.*, arXiv:1110.3401 [astro-ph.IM].